Solid State Commun. 9, 169 (1971).
[31]A. G. Matheson and H. P. Myers (unpublished).
[32]H. Ehrenreich, H. R. Philipp, and B. Segall, Phys. Rev. 132, 1918 (1963).
[33]G. Dresselhaus, M. S. Dresselhaus, and D. Beaglehole, in *Proceedings of the Third Materials Research Symposium* (Natl. Bur. Std., Gaithersburg, Md., to be published).
[34]G. T. Meaden, *Electrical Resistance of Metals* (Plenum, New York, 1965).
[35]B. F. Schmidt and D. W. Lynch, Phys. Rev. B 3, 4015 (1971).

PHYSICAL REVIEW B VOLUME 5, NUMBER 10 15 MAY 1972

Inversion of Fermi-Surface Data Using Partial-Wave Phase Shifts and Their Derivatives: An Application to the Noble Metals*

Jerry C. Shaw, J. B. Ketterson, and L. R. Windmiller
Argonne National Laboratory, Argonne, Illinois 60439
(Received 15 October 1971)

Utilizing the Korringa-Kohn-Rostoker method, we present straightforward procedures for efficiently parametrizing experimental Fermi-surface data. Useful techniques, derived from standard least-squares methods, are generated for fitting areas, cyclotron effective masses, and pressure derivatives of areas, using as adjustable parameters, phase shifts, energy derivatives of phase shifts, and lattice-constant derivatives of phase shifts, respectively. We apply these techniques to recent noble-metal Fermi-surface data and demonstrate that the quality of fit for the above quantities is highly insensitive to the assumed value of the energy parameter used in the formalism.

I. INTRODUCTION

It has recently been suggested by Segal and Ham[1] and demonstrated by Lee[2–4] and Cooke, Davis, and Wood[5] and the present authors[6] that the anisotropy of de Haas–van Alphen (dHvA) data may be accurately parametrized utilizing as adjustable parameters energy-independent partial-wave-scattering phase shifts. The energy-dependent form of the phase shifts, $\eta_l(E)$, characterize the scattering of electrons due to the "muffin-tin" potential used in the augmented-plane-wave (APW)[7] and Korringa-Kohn-Rostoker (KKR)[8,9] methods of calculating electronic dispersion curves.

The advantages of this method are several-fold, but most important is the rapid convergence of the formalism to allow accurate characterization of the data in terms of a few parameters. For example, copper data may be quite accurately fitted using only three phase shifts corresponding to s, p, and d angular-momentum states. This compares with the seven nonphysical parameters used in the Fourier-series techniques[10–12] for the noble metals. For highly distorted surfaces, either Fourier-series techniques[12–14] or, if it is a closed centrosymmetric surface, a series of symmetrized spherical harmonics,[15] require many coefficients to describe the anisotropy of a single sheet. Conceivably, a multiple-sheet Fermi surface can be parametrized using a single set of three or four η_l's; we shall present in a later paper results for fits for such metals, including the effects of spin-orbit coupling.

The energy used to characterize the Fermi surface in this formalism is measured relative to the value of the constant potential in the interatomic region, i.e., $E = E_F - V_{MTZ}$, where E_F is the Fermi energy and V_{MTZ} is the constant potential. Workers have observed a nonunique relationship between the phase shifts and the value of E that give reasonable fits to dHvA data. Preliminary numerical studies[6] suggested that a family of phase shifts versus E could be generated which give accurate fits to dHvA data over a large range of E. Recent attempts to resolve this ambiguity have been made by Andersen[16] and by Heine and Lee.[17] In Sec. III, we give strong numerical evidence to support the contention that the quality of fit to dHvA data is intrinsically E independent and that any E dependence is due to the effects of truncating the order of the secular matrix, i.e., the lack convergence of the formalism resulting from the use of a finite number of phase shifts.

In Sec. II, we describe general techniques, using the KKR formalism, for rapidly determining parameters from a given set of experimental data. In Secs. III–V we describe specific procedures for calculating theoretical quantities, either using a first-principles potential or as functions of adjustable parameters. In each section we present the results of the application of the parametrization schemes to recent data for the noble metals. Finally, in Sec. VI, we present a summary and conclusions, while in the Appendix, we describe straightforward pro-

cedures for determining parameter uncertainties.

II. GENERAL TECHNIQUES

Although what we describe here has been applied using the KKR formalism, the techniques are equally applicable to the APW method. In either case, one is faced with determining the root $E(\vec{k})$ of the determinant of the secular matrix, which for the KKR case is given by[9]

$$\det|\overleftrightarrow{M}| = \det|A_{l,m;\,l',m'}(\vec{k}, E, a) + \sqrt{E}\,\delta_{ll'}\,\delta_{mm'}\cot\eta_l(E,a)| = 0\,, \quad (1)$$

where E is the energy relative to the muffin-tin zero, i.e., $\kappa = \sqrt{E}$ is the electronic wave number in the interatomic region. In subsequent discussions, we will refer to E as the energy parameter. The $A_{l,m;l',m'}$'s are "structure constants"[9,18] which are functions only of E, k vector $\vec{k}$, and lattice constant a, while the effects of the muffin-tin potential are introduced separately through the partial-wave-scattering phase shifts η_l, which are functions only of E and a. The method usually used in determining the relationship between E and $\vec{k}$ is to vary E on some fine grid for a fixed $\vec{k}$ and graphically determine the value of E which gives a root. However, if we diagonalize the secular matrix $\overleftrightarrow{M}$, then its determinant is simply the product of the eigenvalues $\Pi_i\lambda^{(i)}$. Whereas the energy dependence of the determinant is that of a polynomial of the order of the dimensionality of the secular matrix, the eigenvalues are very smooth functions of the energy parameter; thus, it is better to deal with the appropriate eigenvalue rather than the determinant.

For a fixed value of $\vec{k}$, an eigenvalue near zero, say the ith, may be expanded in a Taylor series and the correction to the energy necessary to give a zero eigenvalue predicted by using the Newton-Raphson[19] technique giving

$$\delta E = -\lambda^{(i)}(E)\Big/\left(\frac{\partial\lambda^{(i)}}{\partial E}\right)_{a,\vec{k}}. \quad (2)$$

This process is then iterated until the predicted correction is less than some predetermined value. Similarly, this same procedure may be used in tracing constant E contours. The predicted correction to the $\vec{k}$ vector is given by

$$\delta k_n = -\lambda^{(i)}(\vec{k})/(\vec{\nabla}_k\lambda^{(i)})_{a,E,\vec{\eta}}\cdot\hat{n}\,, \quad (3)$$

where δk_n is the component of the correction along the unit vector $\hat{n}$ and $\vec{\eta}$ is a collection of η_l's. The orbit-tracing procedure has been given elsewhere.[12,13] Since the behavior of $\lambda^{(i)}$ near a root is quite linear, the convergence is very fast, eliminating the need for higher-order terms in the Taylor expansion.

Since $\overleftrightarrow{M}$ is a Hermitian matrix, analytic derivatives for the above procedures may be easily obtained using the Hellman-Feynman theorem.[20,21] The appropriate derivatives are then given by

$$\frac{\partial\lambda^{(i)}}{\partial E} = \sum_{j,l} V_j^{(i)*}\frac{\partial M_{jl}}{\partial E}V_l^{(i)} \quad (4)$$

and

$$(\vec{\nabla}_k\lambda^{(i)})_{a,E,\vec{\eta}} = \sum_{j,l} V_j^{(i)*}\vec{\nabla}_k M_{jl}V_l^{(i)}\,, \quad (5)$$

where $\vec{V}^{(i)}$ is the eigenvector corresponding to the eigenvalue $\lambda^{(i)}$, i.e., $\overleftrightarrow{M}\cdot\vec{V}^{(i)} = \lambda^{(i)}\vec{V}^{(i)}$. It is to be noted that the components of $\vec{V}^{(i)}$ can be used to determine the ratios of the coefficients of the KKR basis functions.

The structure constants are calculated using techniques similar to those used by Davis.[22] Their derivatives with respect to E and $\vec{k}$ are performed analytically. The convergence of the resulting sums are comparable to the structure-constant sums except near a free-electron singularity, in which case, the singularity is squared, thus the same values of the Ewald parameter used in evaluating the structure constants may be used throughout. In general, these sums were carried out to six significant figures.

Orbit tracing is facilitated by the fact that the numerical ordering of eigenvalues for a given $\vec{k}$ corresponds to the numerical ordering of energy levels, i.e., if $\lambda^{(N)}$ corresponds to level n of a numerically increasing set of energy levels, then $\lambda^{(N+1)}$ corresponds to level $n+1$. Thus, in calculating orbit properties of a given sheet, one need only consider the behavior of a $\lambda^{(i)}$ of constant index i for all orbits on that sheet. The computer codes are designed to compute only the ith eigenvalue and eigenvector.[23] For second derivatives with respect to the same or different variables, equations similar to those of second-order-perturbation theory[20] can be developed; however, these require all eigenvectors and eigenvalues of $\overleftrightarrow{M}$. This technique can be used to calculate the elements of the effective mass tensor.

For partial derivatives with respect to other variables taken at constant $\lambda^{(i)}$, one uses the standard rules for differentiating implicit functions. For example, the velocity is given by

$$\vec{\nabla}_k(E) = -(\vec{\nabla}_k\lambda^{(i)})_{a,E,\vec{\eta}}\Big/\left(\frac{\partial\lambda^{(i)}}{\partial E}\right)_{a,\vec{k}}\,, \quad (6)$$

and the derivative of $\vec{k}$ with respect to $\vec{\eta}$ is given by

$$\left(\frac{\partial k_n}{\partial\vec{\eta}}\right)_{a,E,\lambda^{(i)}} = -\left(\frac{\partial\lambda^{(i)}}{\partial\vec{\eta}}\right)_{a,E,\vec{k}} \Big/ [\hat{n}\cdot(\vec{\nabla}_k\lambda^{(i)})_{a,E,\vec{\eta}}]. \quad (7)$$

Likewise, the partial derivative of $\vec{k}$ with respect to lattice constant is given by

$$\left(\frac{\partial k_n}{\partial a}\right)_{\lambda^{(i)}} = -\left(\frac{\partial \lambda^{(i)}}{\partial a}\right)_{\vec{k}} \Big/ \left[\hat{n}\cdot(\vec{\nabla}_k \lambda^{(i)})_{a,E,\vec{\eta}}\right], \tag{8}$$

where k_n is the component of $\vec{k}$ along a specified unit vector $\hat{n}$.

We emphasize again that these same procedures may be utilized for the APW technique and offer computational advantages over other suggested methods,[24] mainly because only one eigenvalue and eigenvector are needed at any one point in the computation. The APW matrix dimensions ($> 30 \times 30$) are, however, considerably greater than the 9×9 usually needed for the KKR formalism.

The procedure outlined above allows considerable automation of both first-principles band calculations and Fermi-surface data fitting. Orbit tracing, cyclotron-mass calculations, volume integrations, and electronic-specific-heat calculations can be carried out efficiently without approximating derivatives by finite-difference techniques or without resorting to interpolation schemes. It also offers derivative information for use in the various interpolation schemes if density-of-states calculations are needed for general energies.

The experimental and calculated quantities in the following discussion are denoted by Q^E and $Q^C(\vec{\alpha})$, respectively, where $\vec{\alpha}$ is a general vector in a parameter space. Since adjusting parameters until the $Q^C(\vec{\alpha})$ most nearly equal the Q^E in the least-squares sense gives the most unbiased estimate of the parameters, regardless of the statistical distribution of the Q^E, we shall adopt the usual mean-square deviation as a measure of the quality of fit. Thus, the quality-of-fit functional is given by

$$\langle \Delta^2 Q(\vec{\alpha})\rangle = \frac{1}{N}\sum_{i=1}^{N} W_i (Q_i^E)^{-2}\left[Q_i^C(\vec{\alpha}) - Q_i^E\right]^2, \tag{9}$$

where N is the number of data points and W_i are weighting factors, usually taken to be inversely proportional to the experimental mean-square percentage deviation of the Q_i^E. For what follows, we shall assume equal weighting and set $W_i = 1$ for all data points.

For determination of the minima in Eq. (9), we determine what values of $\vec{\alpha}$ give a null derivative. Thus, a minimum is determined by the condition

$$\frac{\partial\langle \Delta^2(\vec{\alpha})\rangle}{\partial \vec{\alpha}} = 0 = \frac{2}{N}\sum_{i=1}^{N}\left[Q_i^C(\vec{\alpha}) - Q_i^E\right]\frac{\partial Q_i^C}{\partial \vec{\alpha}}. \tag{10}$$

For iterative calculations, where the Q^C's are nonlinear functions of $\vec{\alpha}$, we wish to expand Q_i^C in a Taylor series about $\vec{\alpha}_0$ (some point near the minima) through terms linear in the correction-vector components and thus predict the vector in parameter space which satisfies the condition set forth in Eq. (10). This gives

$$\overleftrightarrow{T}\cdot\delta\vec{\alpha} + \vec{X} = 0, \tag{11}$$

where

$$\overleftrightarrow{T} = \sum_{i=1}^{N}\left(\frac{\partial Q_i^C}{\partial \vec{\alpha}}\right)_{\vec{\alpha}_0}\left(\frac{\partial Q_i^C}{\partial \vec{\alpha}}\right)_{\vec{\alpha}_0}(Q_i^E)^{-2}, \tag{12}$$

$$\vec{X} = \sum_{i=1}^{N}(Q_i^E)^{-2}\left[Q_i^C(\vec{\alpha}) - Q_i^E\right]\left(\frac{\partial Q_i^C}{\partial \vec{\alpha}}\right)_{\vec{\alpha}_0}, \tag{13}$$

and

$$\delta\vec{\alpha} = \vec{\alpha} - \vec{\alpha}_0. \tag{14}$$

In the case that the Q^C are linear functions of $\vec{\alpha}$, no iterations are required and one gets the above equations with $\vec{\alpha}_0$ set equal to zero. In either case, we can solve for the unknown $\delta\vec{\alpha}$ or $\vec{\alpha}$ by solving a set of linear equations. More general techniques for finding minima of nonlinear functions are available[25]; however, we find that this simple approach suffices for two reasons. First, we are dealing with few parameters. The matrix $\overleftrightarrow{T}$ becomes progressively more "ill conditioned"[26] as we add more parameters and approaches a Hilbert matrix in behavior, becoming quite singular and computationally difficult to handle with as few as five or six parameters. Second, we have found that the elements of $\overleftrightarrow{T}$ are positive definite, a result of the fact that the derivatives of a given area with respect to η_l all have the same sign regardless of l. For nonlinear dependence of Q^C, we are, in effect, approximating the second-derivative matrix by Eq. (12); thus, we can successfully determine a minimum in Eq. (9).

Constraints may be conveniently added to Eq. (11) using the usual Lagrangian-multiplier technique, giving

$$\overleftrightarrow{T}\cdot\delta\vec{\alpha} + \vec{X} + \Lambda\frac{\partial f(\vec{\alpha})}{\partial \vec{\alpha}} = 0, \tag{15}$$

where the parameters are constrained to give $f(\vec{\alpha}) = 0$, and where Λ is to be determined, depending upon the specific constraint. For nonlinear dependences of Q^C on $\vec{\alpha}$, Eq. (15) is to be iterated until the predicted $\delta\vec{\alpha}$ is less than some prescribed value. For the case of linear dependence, $\delta\vec{\alpha}$ is replaced by $\vec{\alpha}$ in Eq. (15) and only one calculation is necessary.

III. AREAS

As discussed in Secs. I and II, areas and their derivatives may be conveniently calculated using the KKR method directly and using Simpsons-rule numerical integration. The calculated area corresponding to the jth experimental area is given by

$$A_j^c(a, E(a), \vec{\eta}(a, E(a))) = \tfrac{1}{2}\int_0^{2\pi} k_\perp^2(\theta)\, d\theta\,, \tag{16}$$

and its derivative with respect to $\vec{\eta}$ is given by

$$\left(\frac{\partial A_j^c}{\partial \vec{\eta}}\right)_{a,E} = -\int_0^{2\pi} \frac{k_\perp^2\,(\partial\lambda^{(i)}/\partial\vec{\eta})_{E,a,\vec{k}}}{\vec{k}_\perp \cdot (\vec{\nabla}_k \lambda^{(i)})_{a,E,\vec{\eta}}}\, d\theta\,, \tag{17}$$

where $\vec{k}_\perp$ is a vector on the Fermi surface and in the plane of the orbit perpendicular to the magnetic field direction used in observing the corresponding experimental area. Here and throughout the remainder of the paper we will use scaled units such that $\vec{k}$ vectors are expressed in units of $2\pi/a$ and energy parameters in units of $(2\pi/a)^2$, with corresponding units for areas and volumes. The elements of the secular matrix are then unitless quantities and, as a result, so are the $\lambda^{(i)}$. As before, $\vec{\eta}$ represents the collection of reduced phase shifts and is in radians. "Reduced" in this sense means that the true phase shift δ_l is given by

$$\delta_l = p_l\pi + \eta_l\,,$$

where $|\eta_l| < \frac{1}{2}\pi$ and where p_l is the number of internal nodes in the solution to the radial Schrödinger equation.

In an analogous fashion, the Fermi volume, that volume contained within the Fermi surface, is given by

$$V(a, E(a), \eta(a, E(a))) = \tfrac{1}{3}\int_0^{2\pi}\int_0^{\pi} k_f^3(\theta, \varphi)\, \sin\theta\, d\theta\, d\varphi\,, \tag{18}$$

while derivatives of V with respect to $\vec{\eta}$ are given by

$$\left(\frac{dV}{d\vec{\eta}}\right)_{a,E} = -\int_0^{2\pi}\int_0^{\pi} \frac{k_f^3(\theta, \varphi)\,(\partial\lambda^{(i)}/\partial\vec{\eta})_{E,\vec{k},a}}{\vec{k}_f \cdot (\vec{\nabla}_k \lambda^{(i)})_{a,E,\vec{\eta}}}\, \sin\theta\, d\theta\, d\varphi\,. \tag{19}$$

Equations (16)–(19) hold for general energy-dependent $\vec{\eta}$'s. If we are interested in adjusting the phase shifts as energy-independent parameters, while constraining the Fermi volume to contain a prescribed number of electrons, i.e., $f(\vec{\eta}) = V(\vec{\eta}) - V_0$, the Lagrangian multiplier of Eq. (15) is then given by

$$\Lambda = \left[V(\vec{\eta}) - V_0 - \left(\frac{\partial V}{\partial \vec{\eta}}\right)_{E,a} \cdot \overline{T} \cdot \vec{X}\right] \Big/ \left[\left(\frac{\partial V}{\partial \vec{\eta}}\right)_{E,a} \cdot \overline{T}^{-1} \cdot \left(\frac{\partial V}{\partial \vec{\eta}}\right)_{E,a}\right], \tag{20}$$

where V_0 for the noble metals is 2 in units of $(2\pi/a)^3$, and where $(\partial V/\partial\vec{\eta}) \cdot \vec{b}$ denotes the dot product $\sum_j (\partial V/\partial\eta_j) b_j$ for a general vector $\vec{b}$.

In Table I we present the results of fitting six experimental dHvA areas for each of the noble metals.[27] The data for copper are those of Coleridge *et al.*,[28] while the data for silver and gold are those of Schirber and O'Sullivan,[29] with the exception of the turning-point areas $TP_{\langle 110\rangle}$. These are obtained by correcting the data of Joseph and Thorsen[30] for silver and Joseph *et al.*[31] for gold. These corrections were determined by shifting the $B_{\langle 100\rangle}$ areas into agreement with the nuclear-magnetic-resonance calibrated data of Schirber and O'Sullivan. The calculations were performed for several different values of the energy parameter. All integrals were calculated using Simpson's-rule numerical integration using $1°-2°$ grids. At a given value of E the η_l's were varied using the techniques described in Sec. II until the predicted change in $\vec{\eta}$ was less than some predetermined value. This usually resulted in values of $\sim 10^{-3} - 10^{-5}$ for the phase-shift derivatives of the error functional. Volumes were calculated by using ~600 vectors in the $\frac{1}{48}$ irreducible wedge of the Brillouin zone.

In Fig. 1 we present values of the root-mean-square (rms) percentage deviation versus assumed values of the energy parameter for the three noble metals using three phase shifts ($l_{\max} = 2$). While shallow minima exist (relative to experimental uncertainty) for silver and gold, quite a pronounced minimum exists for copper. These curves were obtained without invoking the volume constraint. In Table I we present values for the volume [in $(2\pi/a)^3$ units] for three energies. In all three metals the volume exhibits a monotonic decrease with increasing energy. With the exception of silver, the volume passes through the correct value of 2 near the minimum in the rms deviation versus E curves of Fig. 1. In all cases the volume is rather insensitive to the value of E.

The minimum for copper occurs near the value of energy used by Cooke, Davis, and Wood[5] and by Lee.[3] The second energy for copper as listed in Table I (E_{CDW}) corresponds to the value used by Cooke *et al.*[5] By repeating the calculations using $l = 0, 1, 2$, and 3 ($l_{\max} = 3$) phase shifts we find that the minimum corresponds to that value of the energy parameter that gives $\eta_3 = 0$. Indeed, a plot of the type given in Fig. 1 using N phase shifts appears to be nothing more than a measure of the effect of the $N+1$ phase shift not included in the calculation. The three open circles in Fig. 1 show the rms error using $l_{\max} = 3$, while Table II displays values for the phase shifts and the resulting areas. The above contention is confirmed by noting the small shift of the $l = 0, 1$, and 2 phase shifts

upon adding an $l=3$ phase shift for $E=E_{\mathrm{CDW}}$. Such is not the case for $E=0.3$ or 0.9, where shifts are considerably larger. We have not calculated the volumes corresponding to the $l_{\max}=3$ points in view of the insensitivity of the volume to E and in view of the agreement between inverted k vectors for these parameter sets and those corresponding to $l_{\max}=2$ and E_{CDW} for which $V_0=1.9995$. Comparisons between the inverted k vectors are given in Table III. Using a value of 1 part in 10^4 for a representative experimental uncertainty for copper[26] the uncertainties in the η_l were calculated

TABLE I. A comparison of experimental dHvA areas for the noble metals and the corresponding values obtained by the least-squares-fitting procedure described in the text using $l=0,1$, and 2 phase shifts. The lattice constants given by Halse (Ref. 11) were used in converting experimental data to units of $(2\pi/a)^2$. The orbit designations are as follows: B, belly; R, rosette; D, dog bone; N, neck; and TP, turning point [absolute minimum in the area versus field-direction dependence in the (110) plane]. Directions normal to orbit planes are given by subscripts, except $\mathrm{TP}_{\langle 110\rangle}$ where the normal lies in the (110) plane at angles of 16.5, 18.1, and 22.0 deg with respect to $\langle 100\rangle$ for copper, silver, and gold, respectively.

E $(4\pi^2/a^2)$	δ_{rms} $\times 10^3$	η_l $l=0,1,2$ (rad)	V_0 $(8\pi^3/a^3)$	$\mathrm{B}_{\langle 100\rangle}$	$\mathrm{B}_{\langle 111\rangle}$ $(4\pi^2/a^2)$	$\mathrm{R}_{\langle 100\rangle}$	$\mathrm{N}_{\langle 111\rangle}$	$\mathrm{D}_{\langle 110\rangle}$	$\mathrm{TP}_{\langle 110\rangle}$
			Copper						
0.30000 (0.25550 Ry)	0.43	0.76457 0.23413 −0.02189	2.0011	1.8810	1.8238	0.77262	0.06823	0.78769	1.8706
0.690398 (0.58794 Ry)	0.094	0.00670 0.10073 −0.13576	1.9995	1.8821	1.8231	0.77231	0.06823	0.78781	1.8695
0.90000 (0.76643 Ry)	0.34	−0.27521 −0.05255 −0.22944	1.9984	1.8830	1.8225	0.77209	0.06823	0.78794	1.8686
		Expt.[a]		1.88190 (19)	1.82283 (19)	0.772285 (78)	0.068231 (6.3)	0.78722 (78)	1.86948 (19)
			Silver						
0.35000 (0.23367 Ry)	0.78	0.72574 0.21324 −0.02901	2.0002	1.8972	1.8438	0.78632	0.03575	0.80639	1.8864
0.75000 (0.50073 Ry)	0.47	0.000276 0.02913 −0.15435	1.99821	1.8996	1.8433	0.78577	0.03575	0.80662	1.8851
0.90000 (0.60088 Ry)	0.61	−0.19526 −0.08271 −0.22279	1.9972	1.9007	1.8429	0.78553	0.03575	0.80685	1.8843
		Expt.[b,c]		1.9002 (24)	1.8441 (20)	0.7859 (12)	0.03575 (4)	0.8072 (12)	1.8865
			Gold						
0.55000 (0.3679 Ry)	1.3	0.63942 0.21803 −0.12198	2.0036	1.9331	1.7965	0.80085	0.06128	0.77305	1.8809
0.95000 (0.63551 Ry)	0.95	0.02827 −0.05880 −0.33099	2.0008	1.9349	1.7955	0.80023	0.06128	0.77319	1.8779
1.20000 (0.80275 Ry)	1.2	−0.25594 −0.25926 −0.48717	1.9982	1.9362	1.7947	0.7996	0.06128	0.77330	1.8749
		Expt.[b,d]		1.9379 (24)	1.7961 (20)	0.8004 (12)	0.06129 (8)	0.7743 (8)	1.8792

[a]Reference 28. [b]Reference 29. [c]Reference 30. [d]Reference 31.

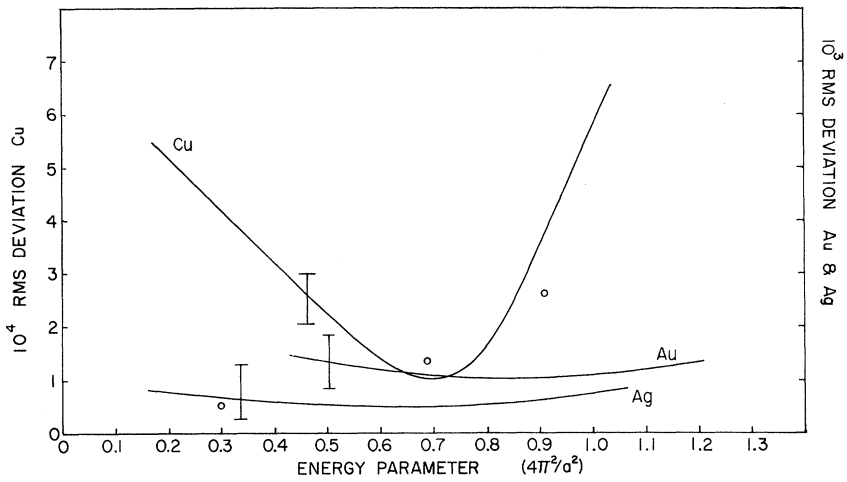

FIG. 1. Plot of the root-mean-square percentage deviation of the areas using $l_{max}=2$ for the three noble metals. The vertical bars represent average experimental uncertainties. The open circles represent rms deviations for $l_{max}=3$ using the η_l listed in Table II. Note the differing scale factors for the three metals. The solid curves were obtained using a grid of approximately 0.05 for the range of E shown for each metal.

using the procedure given in the Appendix. Using these uncertainties gives values of about 0.1% for the k-vector-magnitude uncertainty, however, agreement between orbit radii for different E values is considerably better. Note that at $E=0.3$ the rms uncertainty in the areas approaches 5 parts in 10^5, about the limit of our computational precision, and, in view of the uncertainty in the determination of the lattice constant, it is approaching the limit of meaningful comparison.

It is clear that constraining the volume to accommodate the correct number of carriers is almost unnecessary; indeed, the small deviation from 2 could be taken as experimental verification of charge neutrality. In the case of silver and gold, imposing the constraint has been observed to degrade the quality of fit somewhat; however, in view of the shallowness of the rms error minimum in comparison with the experimental uncertainty, we have not extended parametrization to $l_{max}=3$, awaiting data of the precision of that of copper.

The computational evidence presented so far seems to indicate an intrinsic energy independence of the quality of fit provided adequate convergence is assured. We have used four parameters to fit six pieces of experimental information. If the

TABLE II. A comparison of the calculated areas of copper for fits using $l=0,1,2$, and 3 ($l_{max}=3$) phase shifts. Also given are the areas for a value of $E(E_{CDW})$ near the minimum in the rms error vs E curve of Fig. 1 for fits using $l_{max}=2$. Phase-shift uncertainties were determined by the procedure given in the Appendix. The phase shifts for $l_{max}=3$ correspond to the open circles in Fig. 1.

E $(4\pi^2/a^2)$	η_l $l=0,1,2,3$ (rad)	$B_{\langle 100\rangle}$	$B_{\langle 111\rangle}$	$R_{\langle 100\rangle}$ $(4\pi^2/a^2)$	$N_{\langle 111\rangle}$	$D_{\langle 110\rangle}$	$TP_{\langle 110\rangle}$
0.30000	0.68755 (680)	1.88207	1.82294	0.772302	0.068230	0.787709	1.86950
	0.21989 (120)						
	−0.01946 (22)						
	0.00032 (3)						
0.690398	0.00697 (317)						
(E_{CDW})	0.10082 (124)	1.88213	1.82306	0.772320	0.068232	0.787815	1.86952
	−0.13580 (55)						
	−0.00002 (32)						
0.690398	0.00670	1.88213	1.82305	0.772306	0.068231	0.787811	1.86949
(E_{CDW})	0.10073						
($l_{max}=2$)	−0.13576						
0.90000	−0.26137 (262)	1.88213	1.82308	0.77233	0.068229	0.787824	1.86947
	−0.04461 (133)						
	−0.23333 (72)						
	−0.00458 (73)						
	Expt.[a]	1.88190 (19)	1.82283 (19)	0.772285 (78)	0.068231 (6.3)	0.787722 (78)	1.86948 (19)

[a]Reference 28.

TABLE III. Orbit radii in units of $(2\pi/a)$. These radii are measured from the center of the orbit in a plane normal to the direction given by the subscript of the orbit label. For copper the values of E and η_l ($l_{max}=3$) used are those given in Table II. For silver and gold E and η_l ($l_{max}=2$) values are given in Table I. Halse's (Ref. 11) values for the lattice constants were used in converting experimental data to $(2\pi/a)^2$ units. Angles are measured with respect to the ⟨100⟩ direction.

		Copper			
	Energy	0.30000	0.690398	0.690398 ($l_{max}=2$)	0.90000
$R_{\langle 100\rangle}$	⟨100⟩	0.44984	0.44987	0.44987	0.44991
	⟨110⟩	0.55974	0.55974	0.55974	0.55974
$B_{\langle 100\rangle}$	⟨100⟩	0.82694	0.82692	0.82693	0.82698
	15°	0.78484	0.78483	0.78483	0.78481
	30°	0.75081	0.75088	0.75088	0.75088
	⟨110⟩	0.74321	0.74319	0.74319	0.74316
$N_{\langle 111\rangle}$	⟨110⟩	0.14738	0.14738	0.14738	0.14738
	⟨211⟩	0.14736	0.14737	0.14737	0.14736
$B_{\langle 111\rangle}$	35.26° In (110) plane	0.78244	0.78252	0.78252	0.78256
$D_{\langle 110\rangle}$	⟨001⟩	0.17306	0.17308	0.17307	0.17305
	⟨1$\bar{1}$0⟩	0.67101	0.67104	0.67102	0.67106
	Silver			Gold	
	Energy	0.75		0.95	
$R_{\langle 100\rangle}$	⟨100⟩	0.4366		0.4585	
	⟨110⟩	0.6004		0.5675	
$B_{\langle 100\rangle}$	⟨100⟩	0.8196		0.8777	(0.8753[a])
	15°	0.7868		0.7973	(0.7974[a])
	30°	0.7588		0.7475	(0.7497[a])
	⟨110⟩	0.7530		0.7369	(0.7358[a])
$N_{\langle 111\rangle}$	⟨110⟩	0.1067		0.1397	
	⟨211⟩	0.1067		0.1396	
$B_{\langle 111\rangle}$	35.26° In (110) plane	0.7804		0.7780	
$D_{\langle 110\rangle}$	⟨001⟩	0.1804		0.1223	
	⟨1$\bar{1}$0⟩	0.6612		0.6774	

[a]Reference 12.

number of parameters equals the number of data points, the rms error is, of course, identically zero, therefore we must be careful in evaluating results based on increasing the number of parameters unless we also increase the number of independent data points to obtain a true least-squares fit. Assuming that this criterion has been met, we conclude that any energy dependence of the quality of fit arises from the lack of convergence brought about by truncating the order of the secular matrix.

Additional support in favor of intrinsic energy independence is supplied by the empirical observation of Andersen.[16] He found that a simple transformation from the η_l to the dimensionless $L_l = (r/R_l)\,dR_l/dr - l$, where $R_l(E,r)$ is the solution to the radial Schrödinger equation, leads to the determination of unique information concerning the potential. The relationship between the η_l and the L_l can be shown to be given by

$$L_l(E,r) = -r\kappa\,\frac{n_{l+1}(\kappa r) - \cot\eta_l(E) j_{l+1}(\kappa r)}{n_l(\kappa r) - \cot\eta_l(E) j_l(\kappa r)}\,, \qquad (21)$$

where r is the radius and j_l and n_l are the spherical Bessel and Neumann functions, respectively. It is to be remembered that the energy dependence of the $\eta_l(E)$ is now that brought about by fitting a set of dHvA data at different values of the Fermi level above V_{MTZ}. Thus, the only energy dependence introduced is via the structure constants (i.e., the free-electron propagator or Green's function) and not that of energy-dependent scattering. By plotting the radius dependence of Eq. (21) for different values of E and the corresponding $\eta_l(E)$, one finds a value of r, say S_l, that removes the E dependence of $L_l(E)$. This l-dependent ra-

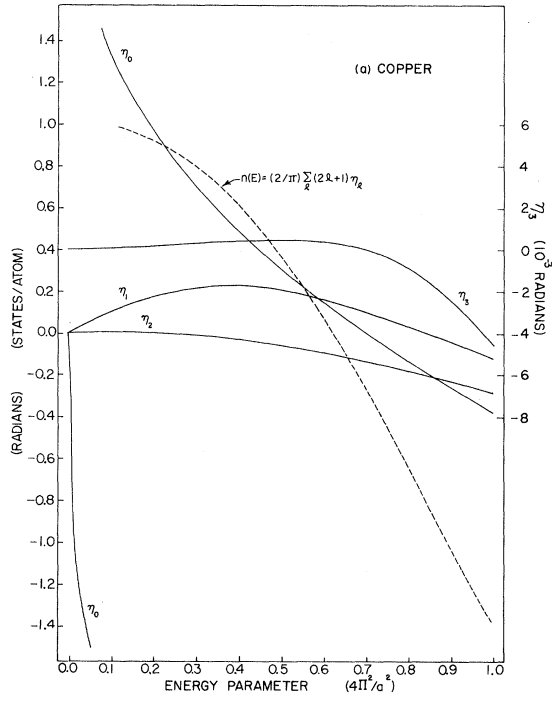

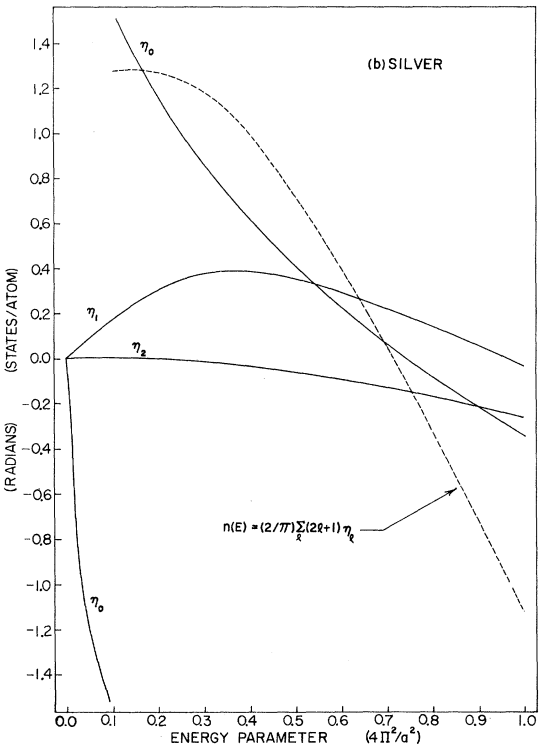

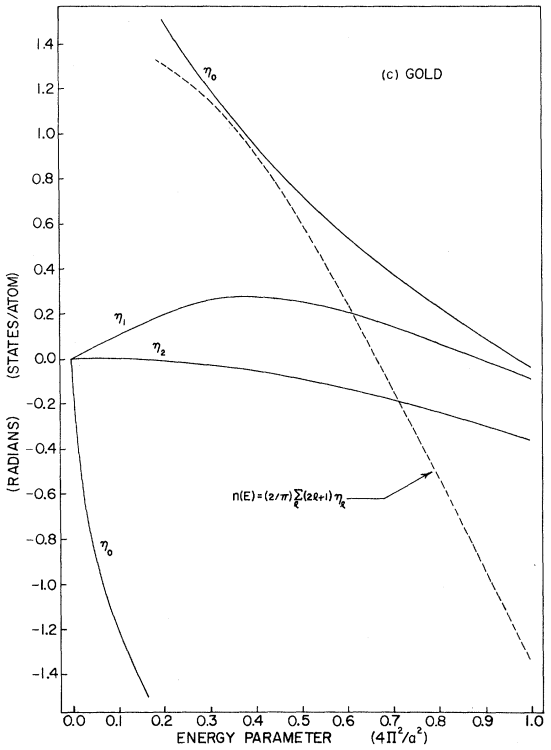

FIG. 2. Plot of $\eta_l(E)$ using Eq. (21) and the values of L_l and S_l given in Table IV. For copper the $l_{max}=3$ values were used, while $l_{max}=2$ values were used for silver and gold. Phase shifts predicted by these curves differ from those in Tables I and II by amounts not resolvable on the scaled used. The Friedel sum is also plotted (states/atom) using the same scale as for the phase shifts (rad).

dius and corresponding $L_l(S_l)$ can be used to predict the E dependence of the η_l by solving Eq. (21) for $\cot\eta_l$. In Fig. 2 we present the E dependence of η_l as determined in this fashion. The f phase shift for copper is plotted using the expanded scale on the right-hand side of Fig. 2. It is to be noted that $\eta_3(E)$ approaches zero for values of E not only near E_{CDW} but also for lower values of E where the rms deviation shown in Fig. 1 is quite large. It is to be noted that the sensitivity of the areas to η_3 at low values of E is quite high, e.g., $\partial A/\partial\eta_3$ at $E=0.3$ is ten times larger than at E_{CDW}. It appears, then, that the deviation of the rms curve from the value at the minimum is roughly proportional to some average over data points of the quantity $\eta_3\ \partial A/\partial\eta_3$.

In Table IV we present values for S_l and L_l for the three noble metals. The values of S_l determined are comparable to the Wigner-Seitz radius S_{WS} (the radius of the sphere of unit-cell volume). Ideally, parametrization schemes should have the property that the addition of more parameters not affect the values of the parameters already determined. We have shown that in the case of the η_l, adding η_3 shifted the η_l of lower l by amounts roughly proportional to the importance of η_3 at that value of E. We note that this shift affects the values of S_l and L_l determined as shown in Table IV for copper. Andersen[16] further proposed that a l-de-

TABLE IV. Values for S_{WS}, S_l, L_l, and α_l for the noble metals. Atomic units are used.

l	S_l	L_l	α_l		
			Copper	$S_{WS}=2.661$	($l_{max}=2$)
0	2.38	−1.48	0.769		
1	2.680	−1.211	0.842		
2	2.965	0.820	2.32		
			Copper	$S_{WS}=2.661$	($l_{max}=3$)
0	2.270	−1.310	0.769		
1	2.643	−1.182	0.845		
2	3.087	0.459	2.24		
3	2.84	−0.558	0.767		
			Silver	$S_{WS}=3.005$	
0	2.66	−1.595	0.706		
1	3.04	−1.149	0.727		
2	3.34	0.708	2.06		
			Gold	$S_{WS}=3.002$	
0	2.580	−2.140	0.805		
1	3.015	−1.279	0.765		
2	3.455	1.457	1.97		

pendent free-electron wave number α_l be defined by setting

$$L_l = -\alpha_l S_l j_{l+1}(\alpha_l S_l)/j_l(\alpha_l S_l),$$

i.e., those values of $\alpha_l S_l$ such that $n_l(\alpha_l S_l)=0$. Values of this parameter are also given in Table IV. It is seen that α_l is less sensitive to the addition of η_3 than are the S_l and L_l.

Values of the Friedel sum rule are also plotted in Fig. 2 for the three noble metals. These curves all follow the general trend of passing through approximately one state per atom for values of $E = E_F - V_{MTZ}$ of roughly one-third the free-electron energy, E_F^0, while approaching zero for $E \approx E_F^0$.[17,32] The values of S_l and L_l given in Table IV may be used to generate the values of $\eta_l(E)$ (as was done for Fig. 2) for use in calculating pseudopotential matrix elements[17,32] using the APW formalism or the Ziman variant of the KKR technique.[33] While the physical and highly qualitative arguments of Heine and Lee[17] shed some light on the origin of the energy independence, the L_l transformation allows the determination of unique parameters concerning the crystalline potential, although it is not clear at this point how this information can be used in a practical calculation involving a first-principles muffin-tin potential. From the viewpoint of inverting experimental data to obtain k vectors, the L_l transformation has considerable utility in aiding the determination of the energy dependence of the quality of fit. Fits at neighboring values of energy can be made in order to determine values of S_l and L_l. From these values the energy dependence of the η_l can be predicted and this information used to determine starting values for further iteration of η_l at energies well removed from the original values. If there is considerable variation in the rms deviation compared to the experimental uncertainties, then the data probably warrant the addition of higher l values.

IV. CYCLOTRON EFFECTIVE MASSES

The cyclotron effective mass, given by $(1/\pi) \times (dA/dE)$, may be calculated from the expression

$$m_j^{*C}(a, E(a), \vec{\eta}(a, E(a))) = -\frac{1}{\pi}\int_0^{2\pi} \frac{k_\perp^2 (\partial\lambda^{(i)}/\partial E)_{a,\vec{k}}}{\vec{k}_\perp \cdot (\vec{\nabla}_k \lambda^{(i)})_{a,\vec{\eta},E}}\, d\theta\,, \tag{22}$$

where we are considering the quantity corresponding to the jth experimental mass. There are two contributions to the energy derivative of $\lambda^{(i)}$ given by

$$\left(\frac{\partial\lambda^{(i)}}{\partial E}\right)_{a,\vec{k}} = \left(\frac{\partial\lambda^{(i)}}{\partial E}\right)_{a,\vec{\eta},\vec{k}} + \left(\frac{\partial\lambda^{(i)}}{\partial\vec{\eta}}\right)_{a,E,\vec{k}} \cdot \left(\frac{\partial\vec{\eta}}{\partial E}\right)_a . \tag{23}$$

The cyclotron mass can then be expressed directly in terms of the phase-shift energy derivatives to give

$$m_j^{*C} = \frac{1}{\pi}\left[\left(\frac{\partial A_j^C}{\partial E}\right)_{a,\vec{\eta}} + \left(\frac{\partial A_j^C}{\partial\vec{\eta}}\right)_{a,E} \cdot \vec{\eta}_E'\right], \tag{24}$$

where

$$\vec{\eta}_E' \equiv \left(\frac{\partial\vec{\eta}}{\partial E}\right)_a$$

Likewise, the energy derivative of the volume is given by

$$\frac{dV}{dE} = \left(\frac{\partial V}{\partial E}\right)_{\vec{\eta}} + \left(\frac{\partial V}{\partial\vec{\eta}}\right)_E \cdot \vec{\eta}_E'. \tag{25}$$

Using the expression for the density of states $n(E) = [2/(2\pi)^3]\,(dV/dE)$ one can compare calculated values of dV/dE to those obtained from specific-heat measurements.

In calculating bare-band cyclotron effective masses, the $(\vec{\eta}_E')_{BAND}$ may be calculated directly from the defining expression for the phase shifts given by Eq. (21) evaluated at R_s, the muffin-tin radius. The energy derivatives of $L_l(R_s, E)$ may be readily obtained.[34] Alternatively, for the purpose of parametrization, the η_E' may be used as adjustable parameters to be used in fitting cyclotron mass and specific-heat data. In this case, the linear dependence of the calculated mass on $\vec{\eta}_E'$ enables one to solve for the $\vec{\eta}_E'$ that give a least-squares fit to the experimental masses by once solving the linear equations defined by Eqs. (11)–(14) with $\vec{\alpha}_0 = 0$. All quantities are to be calculated for the fixed value of $\vec{\eta}$ that gives a best fit to the experimental-

area data, and, as a result, it is a trivial process to carry along the calculation parallel with the area fits.

In fitting mass data, one may wish to constrain the $\vec{\eta}'_E$ to force agreement of dV/dE with the experimental value for the density of states dV_0/dE. For this case, the Lagrangian multiplier in Eq. (15) is given by

$$\Lambda = \left[\left(\frac{dV}{dE}\right)_{\vec{\eta},a} - \frac{dV_0}{dE} - \frac{dV}{d\vec{\eta}} \cdot \overleftrightarrow{T}^{-1} \cdot \vec{X}\right] \Big/ \left(\frac{dV}{d\vec{\eta}} \cdot \overleftrightarrow{T}^{-1} \cdot \frac{dV}{d\vec{\eta}}\right), \quad (26)$$

where

$$f(\vec{\eta}'_E) = \frac{dV}{dE}(\vec{\eta}'_E) - \frac{dV_0}{dE}.$$

In Table V we present a comparison between the experimental cyclotron effective masses for the noble metals and the corresponding values obtained by the least-squares-fitting procedure. For copper, the calculated values fall within the experimental uncertainty of the data of Coleridge and Watts,[36] with the exception of the dog-bone orbit $D_{\langle 110\rangle}$. The quality of fit was not improved upon going to $l_{\max} = 3$. Using the specific-heat data of Martin,[35] we calculate values of dV_0/dE for all three metals. In the copper case, we apply the dV_0/dE constraint, obtaining values for the masses lower than the experimental values by amounts considerably greater than the quoted experimental uncertainty. For silver, the calculated value for dV_0/dE is considerably greater than the experimental value, as is the value obtained by Halse[11] using a Fourier-series inversion scheme. The data for gold were taken from the experimental results of Bosacchi *et al.*[12] and were for angular orientations not lying in symmetry planes. The calculated values given are predicted values for the orientations shown and are compared with calculated values obtained by Bosacchi *et al.*[12] The value for dV_0/dE is 1% lower than the experimental value as compared with the 0.8% lower value obtained by Bosacchi *et al.*[12] using approximately the same data for fitting. The insensitivity of the quality of fit on the assumed value of the energy parameter is again apparent for copper as for the area case. This insensitivity was also observed for silver and gold. In each case, the value of $\vec{\eta}$ used is the same as that used for the area fits. We have not invoked any assumption concerning the "dynamical properties of quasiparticle excitations of the system of interacting electrons in a metal," and yet the interpolation of the experimental cyclotron masses, which contain many-body effects, can be effectively carried out using "bare-band" quantities and the l-dependent parameters $\vec{\eta}'_E$. It is to be noted that the term $(\partial A/\partial E)_{a,\vec{\eta}}$ is by far the dominant term, usually contributing 75% of the total mass. Similarly, the $(\partial V/\partial E)_{a,\vec{\eta}}$ term dominates the specific-heat expression.

The inverted quantities resulting from the mass fits are, of course, the "renormalized" velocities. These quantities may be calculated from Eq. (6) using Eq. (23) and the values for $\vec{\eta}'_E$ contained in Table V. In Table VI we compare values for $\vec{\nabla}_k E$ with those of Lee,[38] Halse,[11] and Bosacchi *et al.*,[12] where we express $\vec{\nabla}_k E$ in free-electron units.

Note that by defining $1 + \lambda(\vec{k}) = v_f^0(\vec{k})/v_f(\vec{k})$,[39] where v_f^0 is the bare-band velocity and v_f is the corresponding renormalized value, we obtain

$$\lambda(\vec{k}) = \frac{\partial \lambda^{(i)}}{\partial \vec{\eta}} \cdot \vec{\Delta}\eta'_E \Big/ \left[\left(\frac{\partial \lambda^{(i)}}{\partial E}\right)_{\vec{\eta}} + \frac{\partial \lambda^{(i)}}{\partial \vec{\eta}} \cdot (\vec{\eta}_E)_{\mathrm{BAND}}\right], \quad (27)$$

where the difference between the experimental and theoretical values of the parameters $\vec{\eta}'_E$ is given by

$$\vec{\Delta}\eta'_E = (\vec{\eta}'_E)_{\mathrm{EXPT}} - (\vec{\eta}'_E)_{\mathrm{BAND}}. \quad (28)$$

This assumes that the energy derivative of the phase shifts $(\vec{\eta}'_E)_{\mathrm{BAND}}$ can be calculated from some l-dependent potential designed to give the $\vec{\eta}$ that are found in Table I for the area fits.

An alternative procedure is to define the cyclotron mass[38] as

$$m^{*C} = \int \frac{1 + \lambda(\vec{k})}{\vec{k}_\perp \cdot \vec{\nabla}_k^{\mathrm{BAND}} E} \, k_\perp^2 \, d\theta, \quad (29)$$

where $\vec{\nabla}_k^{\mathrm{BAND}} E$ is given by

$$\vec{\nabla}_k^{\mathrm{BAND}} E = -(\vec{\nabla}_k \lambda^{(i)})_{a,E,\vec{\eta}} \Big/ \left[\left(\frac{\partial \lambda^{(i)}}{\partial E}\right)_{\vec{\eta}} + \left(\frac{\partial \lambda^{(i)}}{\partial \vec{\eta}}\right)_{\vec{E}} \cdot (\vec{\eta}'_E)_{\mathrm{BAND}}\right],$$

and expand $\lambda(\vec{k})$ in a Fourier series for an open surface, such as copper where translational symmetry[40] is required, or in a series of symmetrized spherical harmonics for a closed surface. For the noble metals, we use the Fourier series

$$\lambda(\vec{k}) = \sum_n C_n S_n(\vec{k}), \quad (30)$$

where the S_n's are sums of $\exp(i\vec{k} \cdot \vec{R}_j)$ over the lattice vectors $\vec{R}_j$ belonging to the nth star appropriate to the fcc lattice. Equation (29) becomes

$$m_i^{*C}(C_n) = \left(\frac{\partial A_i^C}{\partial E}\right)_{\vec{\eta}} + \left(\frac{\partial A_i^C}{\partial \vec{\eta}}\right)_E \cdot (\vec{\eta}'_E)_{\mathrm{BAND}} + \sum_n C_n M_n, \quad (31)$$

where the M_n are given by

$$M_n = \int_0^{2\pi} \frac{(\partial\lambda^{(i)}/\partial E)_{\vec{\eta}} S_n(\vec{k})\, k_\perp^2\, d\theta}{\vec{k}_\perp \cdot (\vec{\nabla}_k \lambda^{(i)})_{a,\vec{\eta},E}} + \int_0^{2\pi} \frac{(\partial\lambda^{(i)}/\partial\vec{\eta})_{a,E} S_n(\vec{k})\, k_\perp^2\, d\theta \cdot (\vec{\eta}'_E)_{\mathrm{BAND}}}{\vec{k}_\perp \cdot (\vec{\nabla}_k \lambda^{(i)})_{a,\vec{\eta},E}} .$$

The masses are now linear functions of the new parameters C_n, while all other quantities are evaluated at the $\vec{\eta}$ that gives a best fit to areas, and the $(\vec{\eta}'_E)_{\mathrm{BAND}}$ are calculated for the adjusted potential that gives the required $\vec{\eta}$. This procedure gives a direct means of calculating the enhancement factor $1+\lambda(\vec{k})$.

We find that, for our purpose, the parametrization directly in terms of the $(\vec{\eta}'_E)_{\mathrm{EXPT}}$ is entirely adequate for interpolating masses in the noble metals as evidenced by the entries of Table V. The success may be fortuitous because of the small enhancement factor for the noble metals. Application to other metals is, of course, needed in order to verify the usefulness of this procedure.

TABLE V. A comparison of experimental cyclotron effective masses for the noble metals and the corresponding values obtained by the least-squares-fitting procedure described in the text. The values of the energy parameters and phase shifts listed in Table I were used in calculating these masses. The masses used in the fit for gold were measured for off-symmetry directions (Ref. 12), thus only predicted values are shown. Also shown are the values of dV_0/dE obtained from specific-heat data (Ref. 35).

E $(4\pi^2/a^2)$	$\vec{\eta}'_E$ $l=0,1,2$ $(a^2\ \mathrm{rad}/4\pi^2)$	dV_0/dE $(2\pi/a)$	$B_{\langle 100\rangle}$	$B_{\langle 111\rangle}$	$R_{\langle 100\rangle}$	$N_{\langle 111\rangle}$ (m^*/m_0)	$D_{\langle 110\rangle}$	$TP_{\langle 110\rangle}$
				Copper				
0.30000	−0.9885 1.14107 −0.07617	···	1.350	1.358	1.305	0.457	1.274	1.332
0.690398	−0.1993 0.4076 −0.01654	6.932	1.353	1.357	1.308	0.456	1.274	1.327
0.690398 (constrained)	−0.1956 0.4082 −0.03800	6.797	1.327	1.325	1.282	0.452	1.253	1.299
0.90000	−0.0551 0.2996 0.0398	6.891	1.356	1.357	1.310	0.456	1.274	1.322
0.90000 (constrained)	−0.0533 0.3001 0.0192	6.797	1.337	1.334	1.292	0.454	1.259	1.303
	Expt.[a,b]	6.797 ± 0.034	1.348 ± 0.015	1.359 ± 0.006	1.305 ± 0.006	0.455 ± 0.006	1.290 ± 0.006	1.321 ± 0.006
				Silver				
0.7500	−0.9534 0.1827 −0.1013	5.222	0.940	0.948	1.072	0.303	1.017	0.929
	Expt.[a,c]	4.940 ± 0.025	0.935 ± 0.005	0.94 ± 0.01	1.08 ± 0.01	0.37 ± 0.01	1.03 ± 0.01	0.93 ± 0.01
	Halse[d]	5.014	0.938	0.940	1.08	0.39	1.031	0.925
				Gold				
0.9500	0.0799 0.3478 −0.3106	5.283	1.147	1.060	1.025	0.2781	0.9756	1.0300
	Expt.[a]	5.338 ± 0.034	···	···	···	···	···	···
	Bosacchi *et al.*[e]	5.295	1.133	1.067	1.013	0.2798	0.9643	1.0362

[a]Reference 35. [b]Reference 36. [c]Reference 37. [d]Reference 11. [e]Reference 12.

V. AREA-PRESSURE DERIVATIVES

In calculating the effects of hydrostatic pressure upon the electronic energy bands of a metal, we need to know the total change in the Fermi energy produced by a change in the lattice constant. Since the Fermi volume must remain invariant under a change of a, the total derivative of V with respect to a must vanish [remembering that V is in units of $(2\pi/a)^3$]. If we consider the volume $V = V(E(a), \vec{\eta}(a, E(a)))$ and calculate the total derivative dE/da using Eq. (25), we get

$$\frac{dE}{da} = -\left(\frac{\partial V}{\partial \vec{\eta}}\right)_{a,E} \cdot \left(\frac{\partial \vec{\eta}}{\partial a}\right)_E \Bigg/ \left[\left(\frac{\partial V}{\partial E}\right)_{a,\vec{\eta}} + \left(\frac{\partial V}{\partial \vec{\eta}}\right)_{a,E} \cdot \left(\frac{\partial \vec{\eta}}{\partial E}\right)_a\right] . \quad (32)$$

If we consider the deformation of a point on the Fermi surface under the constraint that the new $\vec{k}$ still satisfy the secular equation at the new energy, where $\lambda^{(i)} = \lambda^{(i)}(E(a), \vec{\eta}(a, E(a)))$, we obtain, using Eq. (8),

$$\left(\frac{\partial k_\perp}{\partial a}\right)_{\lambda^{(i)}} = \frac{-(\partial\lambda^{(i)}/\partial E)_{a,\vec{\eta},\vec{k}}(dE/da) + (\partial\lambda^{(i)}/\partial\vec{\eta})_{a,E,\vec{k}} \cdot [(\partial\vec{\eta}/\partial a)_E + (\partial\vec{\eta}/\partial E)_a (dE/da)]}{\hat{k}_\perp \cdot (\vec{\nabla}_k \lambda^{(i)})_{a,E,\vec{\eta}}} . \quad (33)$$

Note that the dimensionless $\lambda^{(i)}$ does not explicitly depend upon a.

In complete analogy with previous methods of calculating derivatives of the area with respect to E and $\vec{\eta}$, we can also calculate the area derivative with respect to lattice constant $dA_i/da = \int_0^{2\pi} k_\perp \times (dk_\perp/da)\, d\theta$. Using Eq. (33), we get

$$\frac{dA_i^C}{da} = \left(\frac{\partial A_i^C}{\partial E}\right)_{a,\vec{\eta}} \frac{dE}{da} + \left(\frac{\partial A_i^C}{\partial \vec{\eta}}\right)_{a,E} \cdot \left[\left(\frac{\partial \vec{\eta}}{\partial a}\right)_E + \left(\frac{\partial \vec{\eta}}{\partial E}\right)_a \frac{dE}{da}\right] . \quad (34)$$

The experimental values for dA_i/da may be obtained by using the compressibility $\chi = (-1/V_s) \times (dV_s/dp)$, where V_s is the sample volume; we then get

$$\frac{1}{A_i^E}\frac{\partial A_i^E}{\partial a} = -\frac{3}{a\chi}\frac{1}{A}\frac{dA}{dp} + \frac{2}{a} , \quad (35)$$

where the term $2/a$ accounts for the scaled units of A_i, $(1/A)(dA/dp)$ is the experimental logarithmic pressure derivative and p is the pressure. The quantity $\partial A_i^E/\partial a$ is a measure of the rate of area distortion relative to the Brillouin zone and is zero for the free-electron case.

In calculating dA_i^C/da from "first-principles" potentials, the quantities $(\partial\vec{\eta}/\partial a)_E$ may be calculated by using the Mattheiss[41] procedure by constructing the muffin-tin potential for several different lattice constants. The phase shifts at each lattice constant can be calculated using Eq. (21) and $(\partial\vec{\eta}/\partial a)_E$ determined. If the Fermi volume has been determined at zero pressure, then the quantity dE/da can be calculated, since every quantity in Eq. (32) is known. The area derivatives with respect to lattice constant are then given by Eq. (34).

Alternatively, the $\vec{\eta}_a' \equiv (\partial\vec{\eta}/\partial a)_E$ can be used as adjustable parameters. To facilitate the parametrization, we note that families of η_l versus the energy parameter E, such as in Fig. 2, can be made for a given strain state of the crystal. If we maintain a fixed energy, say E_0, while straining the crystal, then the vertical displacement of a given η_l curve along the E_0 line is given by $\delta\eta_l(E_0) = (\partial\eta_l/\partial a)_{E_0}\delta a$. The corresponding change in the area is then $\delta A = (\partial A/\partial\vec{\eta})_{a,E_0} \cdot (\partial\vec{\eta}/\partial a)_{E_0}\delta a$. Thus, if we take advantage of the insensitivity of the quality of fit (assuming that it still holds for the strained state), then the dE/da term can be set equal to zero. Since E is in units of $(2\pi/a)^2$, this is equivalent to free-electron scaling, which when inserted into Eq. (32) gives the constraint

$$f(\vec{\eta}_a') = \left(\frac{\partial V}{\partial \vec{\eta}}\right)_{a,E} \cdot \vec{\eta}_a' .$$

TABLE VI. Fermi velocities in free-electron units for those values of E, $\vec{\eta}$, and $\vec{\eta}_E'$ listed in Tables I and V. Velocities from the inversions of Halse (Ref. 11), Lee (Ref. 3), and Bosacchi *et al.* (Ref. 12) are also given for comparison.

E $(4\pi^2/a^2)$	Angle from ⟨100⟩ in (100) zone 0°	15°	30°	45°	V_{NECK}
		Copper			
0.30000	0.698	0.772	0.744	0.720	0.413
0.690398	0.687	0.776	0.744	0.714	0.413
0.90000	0.680	0.779	0.744	0.709	0.413
Lee[a]	0.704	0.762	0.722	0.706	0.413
Halse[b]	0.66	0.78	0.74	0.70	0.41
		Silver			
0.75000	1.002	1.106	1.075	1.036	0.366
Halse[b]	0.97	1.11	1.09	1.05	0.35
		Gold			
0.90000	0.726	1.027	0.905	0.811	0.643
Halse[b]	0.80	1.01	0.89	0.85	0.62
Bosacchi *et al.*[c]	0.798	1.033	0.876	0.827	

[a]Reference 3. [b]Reference 11. [c]Reference 12.

TABLE VII. A comparison of the experimental logarithmic pressure derivatives of Schirber and O'Sullivan (Ref. 29) and the corresponding values obtained by the least-squares-fitting procedure described in the text. Also shown are values obtained by the inversion technique of Bosacchi *et al.* (Ref. 14). The values of E and $\vec{\eta}$ used are those given in Table I. Values for the compressibility were taken from Ref. 42 for copper and Ref. 43 for silver and gold.

E $(4\pi^2/a^2)$	$a\eta_a'$ $l=0,1,2$ (rad)	$B_{\langle 100\rangle}$	$B_{\langle 111\rangle}$	$R_{\langle 100\rangle}$	$N_{\langle 111\rangle}$	$D_{\langle 110\rangle}$	$TP_{\langle 110\rangle}$
			($d\ \ln A/dp$ in 10^{-4} kbar^{-1})				
			Copper				
0.30000	0.1096	4.57	4.26	4.61	16.8	4.06	4.48
	−0.3704						
	0.0514						
0.690398	0.1049	4.57	4.27	4.63	16.4	4.07	4.49
	−0.4242						
	0.2036						
0.90000	0.1348	4.57	4.28	4.64	16.3	4.08	4.49
	−0.4119						
	0.2710						
	expt.[a]	4.60 ± 0.2	4.25 ± 0.2	4.30 ± 0.3	18 ± 2	4.0 ± 0.2	
	Bosacchi *et al.*[b]	4.60	4.27	4.31	18.97	4.01	
			Silver				
0.7500	0.5775	5.59	5.18	5.31	61.2	4.76	5.52
	−0.6029						
	0.2914						
	expt.[a]	5.6 ± 0.2	5.1 ± 0.2	5.2 ± 0.3	50 ± 10	4.4 ± 0.3	
	Bosacchi *et al.*[b]	5.61	5.34	5.27	59.8	4.4	

[a]Reference 29. [b]Reference 12.

The Lagrangian multiplier is then given by

$$\Lambda=\left[\left(\frac{\partial V}{\partial\vec{\eta}}\right)_{a,E}\cdot\overleftrightarrow{T}^{-1}\cdot\vec{X}\right]\Big/\left(\frac{\partial V}{\partial\vec{\eta}}\cdot\overleftrightarrow{T}^{-1}\cdot\frac{\partial V}{\partial\vec{\eta}}\right). \tag{36}$$

In Table VII, we give a comparison between calculated logarithmic pressure derivatives of the area obtained by adjusting the $\vec{\eta}_a'$ and the experimental data of Schirber and O'Sullivan.[29] Again, the quality of fit is highly insensitive to the assumed value of the energy parameter.

For the case of gold, we note that the inversion technique fails for $N_{\langle 111\rangle}$ area derivatives in particular. This failure can arise from two possible sources; either the lack of convergence as a result of using only three phase shifts or the failure to include spin-orbit effects. The latter is probably the most reasonable, since the nonrelativistic first-principles calculations of Schirber and O'Sullivan[29] using $l_{\max}=3$ also failed for gold. We shall report, in a later paper, the results for gold, including the effects of spin-orbit splitting.

It is implicit in the above analysis that we are limited to parametrizing linear dependences of the areas upon lattice constant. Using Eq. (33) and the fact that $dE/da=0$, we can calculate the anisotropy of the k vector distortion in this linear approximation. In Table VIII we present values for $(a/k)\,dk/da$ (evaluated at zero pressure) for a limited number of k vectors in the (100) zone, as well as for the neck. These values do not include the effect of free-electron scaling. Due to the poor quality of fit for gold, we have not presented values for this metal. We compare our values for copper with values obtained from the work of Davis, Faulkner, and Joy.[44] These approximate values were obtained by using their tables of k vectors versus lattice constant for the three values of the lattice constant that they used in their work.

VI. SUMMARY AND CONCLUSIONS

In the previous sections we have demonstrated that derivative information may be readily extracted directly from the elements of the secular matrix. We have also shown how this information can be used to give efficient algorithms for parametrizing experimental Fermi-surface data, using phase shifts and their derivatives. The quality of fit resulting from these parametrizations has been shown to be highly insensitive to the assumed value of the energy parameter while still satisfying various constraints.

TABLE VIII. Value for $(a/k)\ dk/da$ using values of the parameters $\vec{\eta}_a'$ given in Table VI. These values do not include the effect of free-electron scaling.

E $(4\pi^2/a^2)$	Angle from ⟨100⟩ in the (100) zone 0°	15°	30°	45°	Neck
			Copper		
0.30000	−0.250	−0.005	+0.152	+0.195	−2.58
0.690398	−0.251	−0.009	+0.146	+0.190	−2.50
0.90000	−0.250	−0.005	+0.145	+0.191	−2.47
Davis *et al.*	−0.300			+0.223	−2.12
			Silver		
0.75000	−0.242	+0.034	+0.236	0.295	−8.97

Using the high-precision dHvA data of Coleridge *et al.*[28] for copper, we have presented the results of careful and accurate numerical studies that suggest that the independence of the quality of fit upon the position of the Fermi level above V_{MTZ} is based on an intrinsic mathematical property of the formalism. It can be concluded that any energy dependence observed in the rms deviation of the areas versus E is due to truncation of the secular matrix.

It has also been shown that cyclotron-effective-mass anisotropy can be characterized by using the energy derivatives of the phase shifts as adjustable parameters. The values of these parameters that give a best fit to the masses were shown to give values of the density of states at the Fermi energy that are in reasonable agreement with experimental values obtained from specific-heat measurements, with the exception of silver where high-precision cyclotron-mass data are not available.

Extending this parametrization philosophy to the area-pressure derivatives has been shown to be straightforward, using the lattice-constant derivatives of the phase shifts as adjustable parameters. Using the derivative information available, it was shown that the rate of change of energy necessary to maintain a constant Fermi volume under a change of lattice constant can be easily calculated. First-principles calculations of the effects of hydrostatic pressure on the Fermi surface can be very easily done without the need for interpolation schemes or finite-difference techniques.

The failure of the nonrelativistic interpolation scheme to account for the area-pressure derivatives in gold is, we believe, rather gratifying in view if the failure of the nonrelativistic first-principles calculation of Schirber and O'Sullivan.[29] Allowing complete freedom of the $d\eta_l/da$ to account for the experimental data allows one to separate the effects of the potential from the effects of, say, adding spin-orbit coupling.

It is now clear that it is possible to define an l-dependent "pseudopotential" that gives the proper scattering phase shifts to fit experimental Fermi-surface areas, the proper energy derivatives of the phase shifts to fit cyclotron-mass data and the proper lattice-constant derivatives of the phase shifts to fit experimental area-pressure-derivative data. The rather limited objective of providing a consistent framework for the complete characterization and inversion of Fermi-surface data has been reached. How the resulting parameters can be used to improve our knowledge of the crystalline potential is yet unclear.

ACKNOWLEDGMENTS

The authors wish to thank Dr. O. K. Andersen for fruitful correspondence and for sending us the results of his work prior to publication. We wish to thank Dr. P. T. Coleridge, Dr. A. A. M. Croxon, Dr. G. B. Scott, and Dr. I. M. Templeton for sending us the results of their dHvA data on copper prior to publication. Thanks also go to Dr. P. T. Coleridge and Dr. B. R. Watts for sending us their cyclotron-mass data for copper prior to publication. We also wish to thank Dr. F. M. Mueller and Dr. J. E. Robinson for stimulating discussions.

APPENDIX

Estimates of parameter uncertainty are easily calculated using quantities already determined in the fitting procedures described in the text. If we assume that the errors incurred in the measurement process are independent, then the rms uncertainty in parameter α_i is given by

$$\delta_{\alpha_i}^{\mathrm{rms}} = \left[\sum_j \left(\frac{\partial \alpha_i}{\partial Q_j^E}\ \delta_{Q_j}^{\mathrm{rms}} \right)^2 \right]^{1/2}, \tag{A1}$$

where $\delta_{Q_j}^{\mathrm{rms}}$ is the experimental uncertainty associated with the Q_j^E. Estimates of $\partial\alpha_i/\partial Q^E$ may be determined by requiring the derivative of the quality-of-fit functional of Eq. (9) to remain zero under small changes in the experimental quanties. We then get the set of linear equations:

$$\vec{\mathbf{X}} + \overleftrightarrow{\mathbf{T}} \cdot \frac{\partial \vec{\alpha}}{\partial Q_i^E} = 0, \tag{A2}$$

where

$$T = \sum_{i=1}^{N} (Q_i^E)^{-2}\ \frac{\partial Q_i^C}{\partial \vec{\alpha}}\ \frac{\partial Q_i^C}{\partial \vec{\alpha}}, \tag{A3}$$

and

$$\vec{\mathbf{X}} = \frac{N}{2}\ \frac{\partial^2}{\partial Q_i^E \partial \vec{\alpha}}\ \langle \Delta^2 Q(\vec{\alpha}) \rangle . \tag{A4}$$

For linear dependence of the Q_i^C on $\vec{\alpha}$, these equations are exact. For nonlinear dependence, we

have neglected the term $\partial^2 Q_i^C/(\partial\alpha_i\partial\alpha_j)$, i.e., we have approximated the second-derivative matrix by (A3).

Once we have the $\delta_{\alpha_i}^{\rm rms}$, we can estimate the uncertainties in the inverted quantities. The rms uncertainty in the k vector, for example, is given by

$$\delta_{\vec{k}}^{\rm rms}=\left[\sum_j\left(\frac{\partial\vec{k}}{\partial\eta_j}\,\delta_{\eta_j}^{\rm rms}\right)^2\right]^{1/2}. \tag{A5}$$

Similarly, uncertainties in the other inverted quantities can be easily calculated if we assume that the parameters are truly independent (zero covariance).

---

*Work performed under the auspices of the United States Atomic Energy Commission.

[1]B. Segall and F. J. Ham, Methods Comput. Phys. 8, 251 (1968).

[2]M. J. G. Lee, Phys. Rev. 178, 953 (1969).

[3]M. J. G. Lee, Phys. Rev. 187, 901 (1969).

[4]M. J. G. Lee, Phys. Rev. Letters 26, 501 (1971).

[5]J. F. Cooke, H. L. Davis, and R. F. Wood, Phys. Rev. Letters 25, 28 (1970).

[6]J. C. Shaw, J. B. Ketterson, and L. R. Windmiller, Bull. Am. Phys. Soc. 16, 314 (1971).

[7]J. C. Slater, Phys. Rev. 51, 151 (1937); T. L. Loucks, *The Augmented Plane Wave Method* (Benjamin, New York, 1967).

[8]J. Korringa, Physica 13, 392 (1947).

[9]W. Kohn and N. Rostoker, Phys. Rev. 94, 1111 (1954).

[10]D. J. Roaf, Phil. Trans. Roy. Soc. (London) A255, 135 (1962).

[11]M. R. Halse, Phil. Trans. Roy. Soc. (London) A265, 53 (1969).

[12]B. Bosacchi, J. B. Ketterson, and L. R. Windmiller, Phys. Rev. B 4, 1197 (1971).

[13]J. B. Ketterson, F. M. Mueller, and L. R. Windmiller, Phys. Rev. 186, 656 (1969).

[14]B. Bosacchi, J. B. Ketterson, and L. R. Windmiller, Phys. Rev. B 2, 3025 (1970).

[15]F. M. Mueller, Phys. Rev. 148, 636 (1966). See also R. L. Aurbach, J. B. Ketterson, F. M. Mueller, and L. R. Windmiller, Argonne National Laboratory Report No. 7659 (unpublished).

[16]O. K. Andersen, Phys. Rev. Letters 27, 1211 (1971).

[17]V. Heine and M. J. G. Lee, Phys. Rev. Letters 27, 811 (1971).

[18]F. S. Ham and B. Segall, Phys. Rev. 124, 1786 (1961).

[19]See any text on elementary numerical analysis, e.g., R. W. Southworth and S. L. Deleeuw, *Digital Computation and Numerical Methods* (McGraw-Hill, New York, 1965).

[20]P. O. Löwdin, J. Mol. Spectry. 13, 326 (1964).

[21]J. W. D. Connolly, *Proceedings of the Third IMR Symposium on the Electron Density of States*, Natl. Bur. Std. Spec. Publ. No. 323 (U.S. GPO, Washington, D.C., 1971).

[22]H. L. Davis, in *Computational Methods in Band Theory*, edited by P. M. Marcus, J. F. Janals, and A. R. Williams (Plenum, New York, 1971), p. 183.

[23]J. W. Givens, Oak Ridge National Laboratory Report No. 1574, 1954 (unpublished); A. S. Householder and F. J. Bauer, Num. Math. 1, 29 (1958). The Givens-Householder algorithim was coded by the Applied Mathematics Division, Argonne National Laboratory and is available as ANL Report No. 150S. This code was modified to return only a specified eigenvalue and eigenvector.

[24]J. H. Wood, in Ref. 22, p. 59.

[25]*Optimization*, edited by R. Fletcher (Academic, London, 1969).

[26]J. H. Wilkinson, *The Algebraic Eigenvalue Problem* (Clarendon, Oxford, 1965), p. 233.

[27]Only one of the three anisotropy parameters used by Lee (Ref. 3) and by Cooke *et al.* (Ref. 5) were used, since the other two areas do not correspond to absolute minima in the area versus field-direction dependence and, as a result, are subject to orientation errors.

[28]P. T. Coleridge, A. A. M. Croxon, G. B. Scott, and I. M. Templeton, J. Phys. E 4, 414 (1971).

[29]J. E. Schirber and W. J. O'Sullivan, Colloq. Intern. Centre Natl. Rech. Sci. (Paris) 118, 113 (1970); Phys. Rev. B 1, 1443 (1970).

[30]A. S. Joseph and A. C. Thorsen, Phys. Rev. 138, A1159 (1965).

[31]A. S. Joseph, A. C. Thorsen, and F. A. Blum, Phys. Rev. 140, A2046 (1965).

[32]M. L. Cohen and V. Heine, Solid State Phys. 24, 37 (1970).

[33]J. M. Ziman, Proc. Phys. Soc. (London) 86, 337 (1965).

[34]See, for example, J. Callaway, *Energy Band Theory* (Academic, New York, 1969), p. 99.

[35]P. T. Coleridge and B. R. Watts, Can. J. Phys. 49, 2379 (1971).

[36]D. L. Martin, Phys. Rev. 170, 650 (1968).

[37]D. G. Howard, Phys. Rev. 140, 1705 (1965).

[38]M. J. G. Lee, Phys. Rev. B 2, 250 (1970).

[39]W. L. McMillan, Phys. Rev. 167, 331 (1968).

[40]We differ with Lee (Ref. 38) who expands $\lambda(\vec{k})$ in spherical harmonics. Since copper is an open surface, $\lambda(\vec{k}+\vec{K}_n)$ must equal $\lambda(\vec{k})$, where $\vec{K}_n$ is a reciprocal-lattice vector. Since each term in a Fourier series is invariant under such an operation, a truncated Fourier series is much more appropriate than a truncated spherical-harmonic series, which is invariant only under the operations of the point group.

[41]L. F. Mattheiss, Phys. Rev. 133, A1399 (1964).

[42]W. C. Overton and J. Gaffrey, Phys. Rev. 90, 969 (1955).

[43]J. R. Neighbors and G. A. Alers, Phys. Rev. 111, 707 (1958).

[44]H. L. Davis, J. S. Faulkner, and H. W. Joy, Phys. Rev. 167, 601 (1968).